J. Fluid Mech. (2008), *vol.* 615, *pp.* 345–369.
doi:10.1017/S0022112008003728 Printed in the United Kingdom

An interactive bypass transition mechanism in wall-bounded flows

F. SEDAT TARDU, RABIA NACEREDDINE AND OLIVIER DOCHE

Laboratoire des Ecoulements Géophysiques et Industriels (LEGI),
BP 53 X 38041, Grenoble, Cédex France
Sedat.Tardu@hmg.inpg.fr

(Received 5 October 2006 and in revised form 15 July 2008)

The interaction between two localized disturbances is analysed in a subcritical channel flow through direct numerical simulations. The initial perturbations are in the form of two pairs of counter-rotating vortices. One of them interacts with the wall-normal vorticity layers set up near the wall, by locally compressing or stretching part of them through the straining motion it induces. The breakdown of spanwise symmetry leads to the rapid development of a new wall-normal vorticity patch that is tilted by the shear and rolls up into a new small-scale streamwise vortex. The process results in a localized turbulent spot at later stages of development. A detailed analysis is carried out to determine the role of different parameters entering the physics of the mechanism. Several critical thresholds that trigger the interactive bypass transition process are found and analysed. The similarity parameters resulting from the parametric investigation coincide well with those governing the self-sustaining Reynolds-shear-stress-producing eddies in the buffer layer of a fully developed turbulent wall flow. It is suggested that the mechanism we propose may play a role in the regeneration cycle of the near-wall turbulence-generating structures by bypassing the three-dimensional streak instability mechanism.

1. Introduction

The disturbance growth and breakdown on time scales shorter than regular Tollmien–Schlichting (TS) waves and their inherent secondary instability process in a subcritical wall-bounded flow is called bypass transition (Morkovin 1969). Nonlinear effects dominate the occurrence of bypass transition for strong enough disturbances.

The bypass mechanism has been intensively investigated both experimentally and through direct numerical simulations. It emanates from non-modal growth mechanisms according to Gustavsson (1991), Butler & Farrel (1992) and Reddy & Henningson (1993). The disturbances originating from non-modal modes are elongated in the streamwise direction and develop into streaky structures almost independently of the initial disturbance (Henningson, Lundbladh & Johansson 1993). The subcritical modes may go through a strong transient growth period before they decay under the viscous diffusion effect, although they are all individually stable. The first stage of this scenario is related to the algebraic growth (lift-up) mechanism (Landahl 1980) resulting from the three-dimensionality. It can be rigorously shown that the zero-streamwise-wavenumber component of the wall-normal vorticity grows linearly in time at the inviscid limit through the integrated effect of the wall-normal velocity. The generation of horizontal velocity perturbations is essentially due to the

lifting up of fluid particles that maintain their streamwise momentum in the presence of the mean shear. The nonlinear growth of the disturbance including the viscous effects is also primarily excited by zero streamwise wavenumber and the resulting turbulent spot is constituted by structures elongated in the streamwise direction, generating inclined near-wall streaks in internal (Henningson *et al.* 1993) or external (Bech, Henningson, Henkes 1998) flows. The streamwise vorticity associated with these streaks rolls up into small-scale streamwise vortices. The subsequent breakdown caused by a rapid increase of the wall-normal velocity near these structures leads to the formation of a local turbulent spot. Well-conducted experiments such as those of Westin *et al.* (1998), Bakchinov *et al.* (1998) and Matsubara *et al.* (2000) have also shown the key role played by the growth of the streaks in triggering the secondary instability prior to the breakdown into spots.

Investigations conducted so far on the bypass transition (BPT) mechanism have involved the effect of local singular perturbations, essentially to investigate the underlying physics. One of the key elements of the BPT process is the generation of wall-normal vorticity. The model we are proposing in the present investigation is based on the interactions of two localized disturbances. They are both individually weak and cannot trigger the BPT, but their combination leads to the generation of wall-normal vorticity and subsequent small-scale vortical structures caused by the strong interactive nonlinearity. The BPT can be triggered for example by local surface irregularities that are far from uncommon in practical situations. Furthermore, the current surface treatment technologies allow the realization of local surface perturbations of desired sizes and spatial distributions. A particular wall distribution of such irregularities could enhance the transition on short time scales. Other applications such as micro-mixing in micro-devices can also be envisaged using a similar strategy. Forcing the interaction between perturbations, such as for example those created by synthetic wall jets, could provide efficient mixing at even very low Reynolds numbers by creating synthetic small-scale turbulent-like structures.

The substructures within a turbulent spot are dynamically similar to the coherent structures regenerated near the wall in a fully developed turbulent flow (see for example Sankaran, Sokolov & Antonia 1998). The investigation of BPT may thus shed light on, somewhat indirectly, the characteristics of the wall turbulence itself. One of the key problems that still exists in wall turbulence is the generation of Reynolds-stress-producing eddies (Hamilton, Kim & Waleffe 1995). The correct understanding of this phenomena is important both from a fundamental and practical point of view since it may lead to the development of efficient strategies for drag and mixing control. The self-sustaining mechanism of wall turbulence is still not entirely understood despite the recent progress (Jiménez 1994; Hamilton *et al.* 1995; Waleffe 1997). The different routes to the generation of self-maintaining quasi-streamwise vortices in the buffer layer are nicely reviewed by Jiménez & Pinelli (1999) but several questions are still unanswered. The regeneration process in the wall turbulence must be related in some way to the pre-existing inner structures, since their birth sequence, commonly called the 'bursting frequency', scales with inner variables, at least at moderately large Reynolds numbers. The key element is the generation of streamwise vorticity zones near the wall that can roll up into distinct quasi-streamwise structures, once sufficient conditions are fulfilled such as concentration and discontinuity in the vorticity distribution (Jiménez & Orlandi 1993). Without a streamwise x-dependent flow field, the stretching, tilting and twisting terms appearing in the production of the streamwise vorticity become zero and the self-sustaining mechanism is broken. The induction of the x-dependence near the elongated streamwise structures should be

partly related to their interaction with the wall flow, i.e. to the structures themselves in conformity with the 'regeneration philosophy'. This is not an easy task, since such dependence is difficult to conceive near elongated structures with lengths larger than the outer scale of the flow. One point of view is that the three-dimensionality of the prevailing shear layer is set up by the undulatory motion of the low-speed streaks, associated with the inflectional instability due to the instantaneous spanwise variations of the fluctuating longitudinal velocity (Swearingen & Blackwelder 1987; Swearingen, Blackwelder & Spalart 1987). Yet the three-dimensional linear streak instability mechanism and the subsequent streak breakdown may also be 'bypassed' through nonlinear connection between the structures themselves in a way similar to the bypass of TS waves. We will show that such interactions are plausible and that close similarity exists with the mechanism we propose and the regeneration of the Reynolds-shear-stress-producing eddies near the wall.

The so-called interactive bypass process we introduce in this investigation is presented in the next section, and the aim of the investigation is outlined in § 3 The details of our direct numerical simulations are given in § 4. Section 5 is devoted first to proving the validity of the regeneration process and then to quantitatively analysing the role of the parameters entering the mechanism. The link between the latter and the self-sustaining coherent structures near the wall of a fully developed turbulent flow is established in § 6.

2. Interactive bypass transition

The details of the bypass transition mechanism that we are considering have been given in Tardu & Nacereddine (2007), based on earlier work of Tardu (1995). A detailed outline will be provided here for completeness.

In the late stages of the bypass transition mechanism, a single perturbation of sufficiently high intensity leads to small-scale quasi-streamwise vortices similar to the coherent structures found in the buffer layer of a fully developed turbulent wall flow (Henningson *et al.* 1993). Triggering streamwise vorticity through some specific interactions between localized structures should, therefore, enhance the transition. The transport equation of the streamwise vorticity ω_x is given by

$$\frac{\partial \omega_x}{\partial t}+(U+u)\frac{\partial \omega_x}{\partial x}+v\frac{\partial \omega_x}{\partial y}+w\frac{\partial \omega_x}{\partial z}=\omega_x\frac{\partial u}{\partial x}-\frac{\partial w}{\partial x}\left(\frac{\partial U}{\partial y}+\frac{\partial u}{\partial y}\right)+\frac{\partial v}{\partial x}\frac{\partial u}{\partial z}+\nu\nabla^2\omega_x, \quad (1)$$

in a Poiseuille flow subjected to three-dimensional perturbations. Hereafter x, y and z are respectively the streamwise, wall-normal and spanwise coordinates with corresponding velocity components u, v and w. The fluctuating vorticity components in the x-, y- and z-directions are denoted ω_x, ω_y and ω_z. The mean velocity distribution of the Poiseuille flow is $U(y)$, and u, v and w depend on x, y, z and the time t, while ν is viscosity. The net contribution to the production of the tilting and twisting of the wall-normal and spanwise vorticity components reduces exactly to

$$\omega_y\left(\frac{\partial U}{\partial y}+\frac{\partial u}{\partial y}\right)+\omega_z\frac{\partial u}{\partial z}=-\frac{\partial w}{\partial x}\left(\frac{\partial U}{\partial y}+\frac{\partial u}{\partial y}\right)+\frac{\partial v}{\partial x}\frac{\partial u}{\partial z}.$$

A simple order-of-magnitude analysis shows that the leading production term during the transient period of the bypass process is

$$-\frac{\partial w}{\partial x}\left(\frac{\partial U}{\partial y}+\frac{\partial u}{\partial y}\right)\approx-\frac{\partial w}{\partial x}\frac{\partial U}{\partial y},$$

which originates from the tilting of the wall-normal vorticity ω_y by the shear. The dominant ω_x production term in the fully developed turbulent wall layer is the same (Sendstad & Moin 1992) and at the same time it plays a key role in the linear instability of the streaks (Asai, Minagawa & Nishioka 2002, p. 306). The triggering of compact zones with high $-\partial w/\partial x$ concentration is therefore a key element not only in the bypass transition mechanism but also in the regeneration of the near-wall coherent structures. Because of its importance this specific part of the wall-normal vorticity $\omega_y = \partial u/\partial z - \partial w/\partial x$ will be denoted by $\omega_y^* = -\partial w/\partial x$ hereafter.

We will first establish the general conditions leading to the setting-up of compact ω_y^* zones and subsequently present a related conceptual model. Given a vorticity field $\boldsymbol{\omega}$, the associated rotational velocity field is

$$\boldsymbol{u}(\boldsymbol{x}, t) = -\frac{1}{4\pi} \int \frac{(\boldsymbol{x} - \boldsymbol{x}') \wedge \boldsymbol{\omega}(\boldsymbol{x}', t)}{|\boldsymbol{x} - \boldsymbol{x}'|^3} \, \mathrm{d}V(\boldsymbol{x}'), \tag{2}$$

according to the Biot-Savart law. Here, $||$ stands for the norm of the vector, $\boldsymbol{u} = (u, v, w)$, $\boldsymbol{\omega} = (\omega_x, \omega_y, \omega_z)$ and $\mathrm{d}V$ is the infinitesimal volume element. Suppose that there is a vorticity gradient $\partial\boldsymbol{\omega}(\boldsymbol{x}', t)/\partial x'$ at a given time t in some region R. The induced velocity gradient is computed by differentiating (2) and integrating by parts (Jiménez 1992). This gives explicitly

$$\frac{\partial w}{\partial x}(x, y, z, t) = -\omega_y^* = -\frac{1}{4\pi} \int_R \frac{(x - x')\dfrac{\partial \omega_y}{\partial x'} - (y - y')\dfrac{\partial \omega_x}{\partial x'}}{[(x - x')^2 + (y - y')^2 + (z - z')^2]^{3/2}} \mathrm{d}x' \mathrm{d}y' \mathrm{d}z'. \tag{3}$$

The integration is carried out over all the volume of fluid in which there is any gradient $\partial\omega_y/\partial x$ or $\partial\omega_x/\partial x$ that can both trigger concentrated ω_y^* zones. We will deal here with the effect of $\partial\omega_y/\partial x$ created by interactions of elongated streamwise structures. Such interactions play an important role in the regeneration of the Reynolds-shear-stress-producing eddies in the buffer layer of a fully developed turbulent wall flow (Brooke & Hanratty 1993; Bernard, Thomas & Handler 1993; Tardu 1995). Consider, to this end, the conceptual model given in figure 1 that shows two pairs of counter-rotating vortices labelled respectively A and B. Normal-vorticity ω_y layers are generated behind the vortices, resulting from the kinematics induced by the near-wall velocity distribution. This is of observed in the direct numerical simulations Jiménez (1994) and can be easily understood through figure 1. A single quasi-streamwise vortex generates respectively a high-speed $u > 0$ streak in the sweep part of the induced near-wall flow and a low-speed streak $u < 0$ on the ejection side. The wall-normal vorticity is $\omega_y = \partial u/\partial z - \partial w/\partial x$ near the wall and in the neighbourhood of elongated structures reduces to $\omega_y \approx \partial u/\partial z$. It appears essentially as 'the sidewalls of the high- and low-speed streaks' at a certain time and location, as reported by Jiménez & Moin (1991). This is shown schematically in figure 1 where layers of positive and negative vorticity are denoted by ω_{y+} and ω_{y-} respectively.

Assume now that there is a streamwise variation in the vorticity associated with the wall-normal ω_{y+} and ω_{y-} layers induced by the mother eddy A and concentrated respectively at $z < 0$ and $z > 0$ of the domain shown in figure 1. The induced $\partial w/\partial x$ for this configuration is

$$\frac{\partial w}{\partial x}(x, y, z, t) = -\frac{1}{4\pi} \int_{-\infty}^{\infty} \int_{-\infty}^{\infty} \int_{z'=0}^{\infty} (x - x') F \, \mathrm{d}x' \, \mathrm{d}y' \, \mathrm{d}z', \tag{4}$$

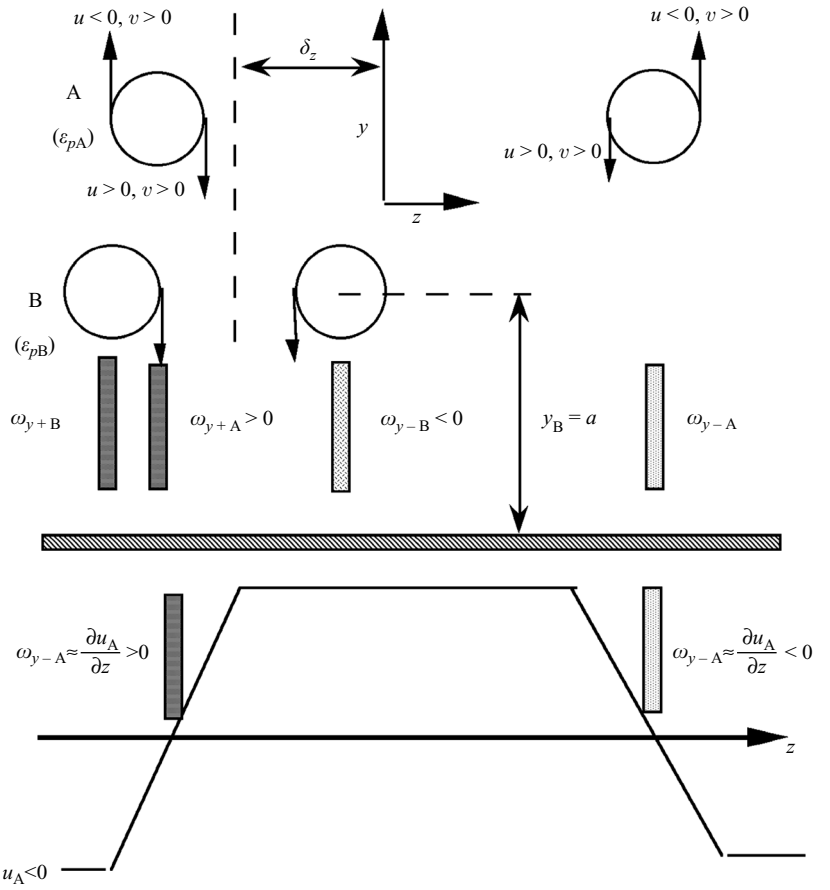

FIGURE 1. Cross-sectional view of two pairs of counter-rotating quasi-streamwise vortices in the plane y, z. The pair A generates wall-normal vorticity layers denoted by $\omega_{y\pm A}$ that are positive and negative respectively the left and the right. The pair B generates similar vorticity layers. The left vortex of the pair B interacts by compression with ω_{y+A} and is rapidly destroyed. That creates an asymmetry in the development of $\omega_{y\pm A}$ and generates new streamwise vorticity layers.

where

$$F = \frac{\partial \omega_{y+}/\partial x'}{[(x-x')^2+(y-y')^2+(z+z')^2]^{3/2}} - \frac{|\partial \omega_{y-}/\partial x'|}{[(x-x')^2+(y-y')^2+(z-z')^2]^{3/2}}.$$

The average $\langle \partial w/\partial x \rangle$. generated between ω_{y+} and ω_{y-} layers over any spanwise-symmetrical surface S at a given wall-normal distance y is

$$\left\langle \frac{\partial w}{\partial x} \right\rangle = -\frac{1}{4\pi S} \int_S \int_R G \, \Delta \, \mathrm{d}x' \, \mathrm{d}y' \, \mathrm{d}z' \, \mathrm{d}S, \tag{5}$$

where

$$G = (x-x') \left[\frac{1}{[(x-x')^2+(y-y')^2+(z+z')^2]^{3/2}} - \frac{1}{[(x-x')^2+(y-y')^2+(z-z')^2]^{3/2}} \right]$$

and

$$\Delta = \frac{\partial \omega_{y+}}{\partial x'} - \left| \frac{\partial \omega_{y-}}{\partial x'} \right|.$$

The concentration of the new vorticity ω_y^*, its tilting and subsequent roll-up into a new quasi-streamwise structure depend directly on the intensity of the asymmetry Δ.

Presumably, when an asymmetry appears in the distribution of the ω_y layers surrounding the flow induced by the mother eddy A, a local ω_y^* is introduced and the x dependence starts in the plane (x, z). The compression of one of the $\omega_{y\pm A}$ layers by the large positive straining induced by the left counter-rotating vortex B shown in figure 1 may break the symmetry and trigger ω_y^*. To show this possibility, consider the evolution of $\omega_{y\pm A}$. Assuming that this evolution is approximately x-dependence free during the early stage of the regeneration process then

$$\frac{\partial \omega_y}{\partial t} + v\frac{\partial \omega_y}{\partial y} + w\frac{\partial \omega_y}{\partial z} = -\frac{\partial U}{\partial y}\frac{\partial v}{\partial z} + \nu\left(\frac{\partial^2 \omega_y}{\partial y^2} + \frac{\partial^2 \omega_y}{\partial z^2}\right), \tag{6}$$

where the stretching of the normal vorticity $((\partial u/\partial z)(\partial v/\partial y))$ has been neglected compared with the lifting of the spanwise vorticity $(-(\partial U/\partial y)(\partial v/\partial z))$. Next consider the compression effect of the 'triggering eddy' B on ω_{y+A} (figure 1). The vortex structure B acts as a single point vortex with a Reynolds number Re_B, located at $y_B = a$. The inviscid flow induced by the vortex and its image have two stagnation points at $z_{sB} = \pm\sqrt{3}\, y_B$ which are located on the sweep and ejection sides (Doligalski & Walker 1984). The strain induced at these points is $\gamma_B^+ = \pm\sqrt{3}Re_B/4a^{+2}$ where superscript + stands for quantities non-dimensionalized by the viscosity ν and a reference velocity U_c. The vortex Reynolds number is defined as $Re_B = \Gamma_B/(2\pi\nu)$, Γ_B being the associated circulation. Figure 1 shows that the stagnation flow on the sweep side of B interacts with the tail of the ω_{y+A} distribution. In the interaction zone the wall-normal scale is significantly smaller than the spanwise one. Therefore, in this region the spanwise diffusion may be neglected compared with the wall-normal one. Accordingly, the non-dimensional equation governing ω_{y+A} layer near the stagnation point is

$$\frac{\partial \omega_{y+A}^+}{\partial t^+} - \gamma_B^+ y^+ \frac{\partial \omega_{y+A}^+}{\partial y^+} = \frac{\partial^2 \omega_{y+A}^+}{\partial y^{+2}}. \tag{7}$$

This equation describes the development of a Burgers vortex sheet whose asymptotic thickness is determined by the balance between the compression of the vortex layer and the diffusion. The general similarity solution for a time-dependent strain is given by Corcos & Sherman (1984, pp. 61–62). For a constant strain it takes the form

$$\omega_{y+A}^+ \propto \frac{\exp(-\gamma_B^+ t^+)}{\sqrt{\pm\exp(-2\gamma_B^+ t^+)\left(\delta_{iA}^{+2} - \delta_a^{+2}\right) + \delta_a^{+2}}}. \tag{8}$$

In this relationship $\delta_a^+ = \sqrt{\pi/(2\gamma_B^+)}$ is the asymptotic thickness of the ω_{y+A} layer subject to the steadily positive strain γ_B^+. The choice of $\pm$ depends on whether the initial thickness δ_{iA}^+ is larger or smaller than δ_a^+. In the first case the compression will concentrate the vorticity, while, in the second, the thickness of the vorticity layer will increase up to δ_a^+ under the dominating diffusion effect. The asymptotic thickness is reached in a time of about

$$t^+ \approx \left[\left(\frac{2\delta_{iA}^{+2}}{\pi}\gamma_B^+\right)^{\pm 1} - 1\right]^{1/2} \frac{1}{\gamma_B^+}.$$

For larger times the local vorticity disappears exponentially in time according to $\omega_{y+\mathrm{A}} \propto \exp(-\gamma_{\mathrm{B}}^{+} t^{+})$. The negative $\omega_{y-\mathrm{A}}$, on the other hand is located far away from the stagnation flow. It is primarily under the effect of viscosity. The maximum vorticity in this layer decreases, therefore, as $\omega_{y-\mathrm{A}} \propto 1/\sqrt{t^{+}}$. This implies that for $t^{+} \gg 2/\gamma_{\mathrm{B}}^{+}$ the positive sidewall disappears almost instantaneously giving rise to a zone of concentrated $\Delta = \partial\omega_{y+}/\partial x' - |\partial\omega_{y-}/\partial x'|$ and subsequently to the generation of $\omega_{y\,n}^{*} = -\partial w/\partial x$. Hereafter the subscript n in $\omega_{y\,n}^{*}$ refers to the new $-\partial w/\partial x$ layers induced by interaction. The $\omega_{y\,n}^{*}$ generated is of opposite sign to the compressed layer $\omega_{y+\mathrm{A}}$.

Note that, incidentally and depending on the spanwise shift δ_z of B with respect to A, wall $\omega_{y\pm\mathrm{A}}$ layers can interact with the ejections induced by B. Then, the compression becomes stretching and intensifies one of the sides $\omega_{y\pm\mathrm{A}}$, creating Δ and regenerating fresh $\omega_{y\,n}^{*}$ zones. The mechanism is therefore essentially similar in this case, even though from a purely fundamental point of view the stretching is not just the opposite of compression. The analysis conducted here is conceptual and analytical solutions are outside the scope of this paper. Direct numerical simulation experiments are used to show the validity of the suggested mechanism.

3. Aim of this investigation

The generation of new structures is related to the effect of the primary ones by means of an interaction with existing wall-normal vorticity layers by a somewhat deterministic scenario, according to the mechanism proposed in the previous session. This is certainly not a unique way to generate structures and enhance the bypass transition mechanism. The source term $-(\partial w/\partial x)(\partial U/\partial y)$ contributes only in a limited manner to the creation of elongated streaks, and the advection term $v\partial\omega_x/\partial y$ plays also an important role in the genesis of new structures according to Hamilton *et al.* (1995). Yet the scenario we propose has the merit of connecting the regeneration process to pre-existing structures and may have some repercussions on both the bypass transition and the near-wall coherent-structure regeneration processes. Although there are several contributions in the literature on streak breakdown, and some qualitative arguments inferred from direct numerical simulations (Brooke & Hanratty 1993), there is still a lack of simple physical models, in particular dealing with the early stages of the $\partial w/\partial x$ shear layer regeneration. Most of the time, one is confronted with the complexity caused by the incoherent turbulence and difficulties in the identification of the coherent events near the wall. Thus, indirect investigations using, for example, the flow field induced by a stochastically estimated hairpin vortex (Adrian 2007) can give valuable information on the wall turbulence structure. The aim of the present investigation is to check the validity of the hypotheses made in the previous section through a detailed parametric study by using direct numerical simulations (DNS) in a channel flow. The details of the DNS together with the initial conditions we use will be discussed in the next section. Section 5 will present the results, first showing qualitatively the validity of the proposed mechanism followed by a quantitative analysis.

4. Direct numerical simulations and initial conditions

The channel direct numerical simulations code of Orlandi (2001) has been modified and adapted for the present purpose. The code is of finite-difference type combined with fractional-step procedure. The nonlinear terms are explicitly resolved

by an Adams–Bashforth scheme. Periodical boundary conditions are used in the homogeneous streamwise and spanwise directions. The number of computational modes is $256 \times 128 \times 128$ in the streamwise, wall-normal and spanwise directions. The size of the computational domain extends $16\pi h$ in x, $2h$ in y and $8\pi h$ in z where h is the half-height of the channel. Stretched coordinates are used in the wall normal-direction. Hereafter quantities are normalized with respect to h and the centreline velocity of the Poiseuille base flow. To give an idea of the grid sizes, consider a fully developed turbulent flow at $Re = 2000$ at which the majority of computations here are performed. The grid sizes in wall units, scaled by the viscosity and the shear velocity, are $\Delta x^+ = \Delta z^+ = 17$ and the first mesh point is situated at 0.1 from the wall. This is to be compared with Henningson *et al.* (1993) who used $\Delta x^+ = 67$ and $\Delta z^+ = 17$ for their moderate-perturbation-amplitude case, which is close to the present investigation. We tested the resolution by performing one computational set with $512 \times 128 \times 512$ modes, and found no significant effect of the grid sizes on the results.

Two pairs of counter-rotating vortices were injected in the channel flow with stream functions of the form

$$\psi = \varepsilon\, f(y)(x'/l_x)\, z' \exp\left[-(x'/l_x)^2 - (z'/l_z)^2\right], \tag{9}$$

where $x' = x\cos\vartheta - z\sin\vartheta$, $z' = x\sin\vartheta - z\cos\vartheta$ and ϑ is the angle of the perturbation which has been set to $\vartheta = 0$ here. The perturbation flow field is given by

$$(u, v, w) = (-\psi_y \sin\vartheta, \psi_{z'}, -\psi_y \cos\vartheta) \tag{10}$$

and

$$f(y) = (y)^p (2 - y)^q, \tag{11}$$

where y is the distance from the upper wall ($y = 0$; $y = 1$ corresponds to the centreline). The initial induced streamwise perturbation velocity component u is uniformly zero in the whole domain. This is the same type of perturbation as used by Henningson *et al.* (1993). The difference here is in the modelling of the configuration given in figure 1. We have combined two different ψ for the structures A and B and shifted B in the z-plane. The streamfunction corresponding to the structure B is of the same form but shifted in the spanwise direction by δ_z, i.e.

$$\psi_B = \varepsilon_B\, f_B(y)\,(x'/l_x)(z' + \delta_z) \exp[-(x'/l_x)^2 - (z' + \delta_z/l_z)^2]. \tag{12}$$

The perturbation parameters and p and q are chosen in such a way that B is closer to the wall and interacts sufficiently strongly with the wall vorticity layers generated by A. The imposed streamfunction is $\psi_A + \psi_B$. The Reynolds number based on the centreline velocity and half-height is $Re = 2000$ throughout the whole study. Recall that the critical Reynolds number of the Poiseuille flow is $Re_c = 5772$. The Re we are investigating here is significantly smaller than in Henningson *et al.* (1993) to emphasize the subcritical nature of the bypass transition mechanism.

5. Results

5.1. *Interactive bypass transition*

The intensities ε_A and ε_B appearing in the perturbation stream functions, (9) and (12), are chosen in such a way that A and B cannot individually trigger the bypass transition alone. The structure A is at the centreline $y_A = 1$ and $p_A = q_A = 2$. Its streamwise and spanwise extends are $l_{xA} = l_{zA} = 4$. The pair of counter-rotating vortices B are placed

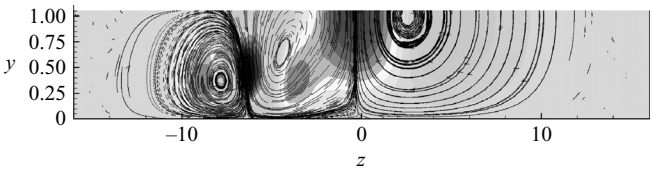

FIGURE 2. Initial wall-normal velocity distributions at $x = 2$ corresponding to the configuration given in figure 1. The structure A is centred at $y = 1$ (centreline) and B at $y = 0.4$. The spanwise shift between A and B is $\delta_z = 6$.

closer to the wall at $y_B = 0.4$ by monitoring the parameters $p_B = 1.5$ and $q_B = 6$ appearing in the function $f_B(y)$ of (12). The characteristic length scales of B are half those of A with $l_{xB} = l_{zB} = 2$. We found that the perturbation intensities that destabilize the flow for each individual structure are respectively $\varepsilon_A = 0.3$ and $\varepsilon_B = 0.05$ under these circumstances. Thus, we have chosen $\varepsilon_A = 0.1$ and $\varepsilon_B = 0.02$ that are three times smaller to ensure that the bypass transition is not triggered by A or B alone. The spanwise shift δ_z between A and B is fixed for the moment at $\delta_z = -6$ to reproduce the situation given in figure 1.

Figure 2 shows the initial wall perturbation velocity contours in the (y, z)-plane at $x = 2$. The topology of the perturbed flow field is strikingly different in the interaction zone $z < 0$ compared to $z > 0$. The strain exerted by B near the spanwise shift $z = \delta_z = -6$ is also clearly perceptible in this figure.

The temporal evolution of the total energy

$$E_{tot} = \iiint_V (u^2 + v^2 + w^2)\,\mathrm{d}V$$

computed in the whole computational volume V is shown in figure 3. It is divided by the initial perturbation energy $E_{tot\,0}$. It is seen that E_{tot} increases exponentially at $t > 100$ when A is combined with B, while the individual energy associated with A and B decreases to zero after the algebraic stage. Figure 4 compares the wall-normal velocity v contours at $t = 120$ generated by A + B to those corresponding to B alone. The results for A alone are not presented because the structure B, which is closer to the wall, is the most critical in terms of triggering the flow. The structure B induces extremely weak perturbations, but the interaction of B with A generates an extended zone of v with the appearance of small-scale structures of high intensity. The latter are centred at $z = \delta_z = -6$ where the stretching of the wall-normal vorticity layer ω_{y+A} is significantly large (figure 1). Note the total absence of activity at $z \geqslant 0$, where the effect of asymmetry is non-existent. Only the combination of A with B in a way specific to the mechanism, we suggest, leads to the generation of a turbulent spot.

The $\partial w/\partial x$ contours at $x = 40$ and $t = 120$ are shown in figure 5(a). An intense inclined $\omega^*_{y\,n} < 0$ layer is clearly perceptible extending from $z \approx -9$ and $y \leqslant 0.25$ in close agreement with the mechanism suggested in figure 1. Figure 5(b) shows the streamwise vorticity ω_x contours at the same location and time. Two freshly rolled up small-scale quasi-streamwise vortices are clearly seen near the wall. They result from the tilting of concentrated $\omega^*_{y\,n}$ regions by the mean shear. Detailed analysis of the data revealed that the tilting process takes place as early as $t \approx 12$. Vorticity should of course not be confused with vortices, but analysis of the λ_2 contours (Jeong & Hussain 1995) used to detect the quasi-streamwise vortices revealed effectively the occurrence of the roll-up at this stage (see figure 7 discussed below).

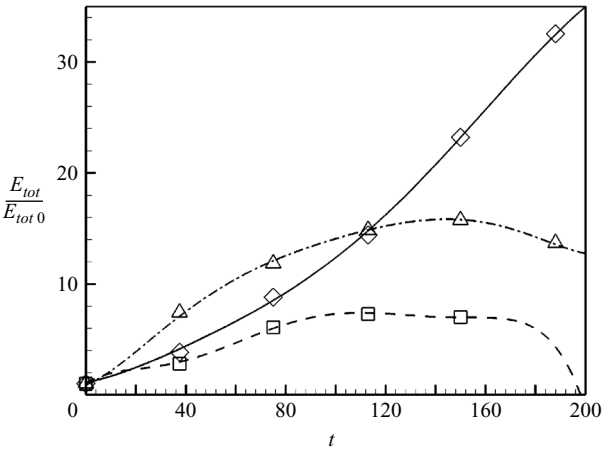

FIGURE 3. Temporal evolution of the total energy for the interaction A + B, and A and B only. —◇—, A+B; ——□——, A; — —△— —, B.

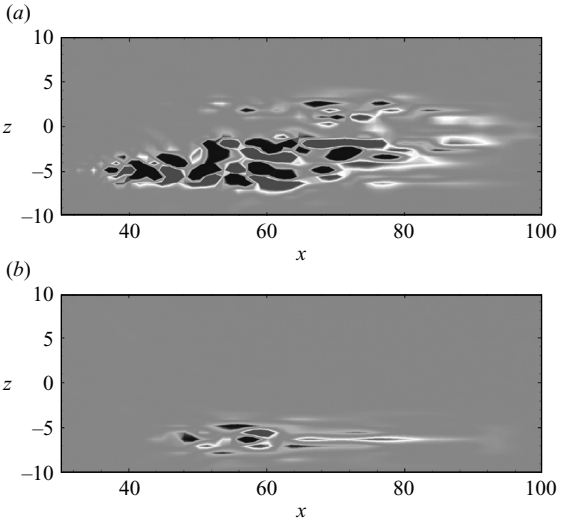

FIGURE 4. Wall-normal velocity v contours at $t = 120$ and $y = -0.6$ corresponding to structures (*a*) A + B and (*b*) B alone. Minimum and maximum levels in (*a*) are +0.7 (darker zones) and −0.7 (lighter regions). The maximum and minimum in (*b*) are only ±0.1.

The details of the generation mechanism are provided in a video that is available on request. The straining sweep event generated by B (figure 1) cuts the ω_{y+A} layer into a pitchfork structure and the compressed layer leads to a rapid ejection from the wall of an intense new $\omega^*_{yn} > 0$ zone after only $8h/U_c$. Figure 6 shows the $\partial w/\partial x$ contours at $t = 10$. The freshly generated ω^*_{yn}, coloured in yellow, appears suddenly as a thin vorticity wall layer extending to nearly the channel centreline. It is situated near the stagnation point induced by B at $z = -6$, once more in agreement with the mechanism proposed here. It should be emphasized that the process being discussed here is structurally different from the genesis mechanism proposed by the Lehigh group (Smith *et al.* 1991). It that case, it is known that when a streamwise vortex approaches the wall it creates a new vorticity layer of opposite sign (Walker 1989).

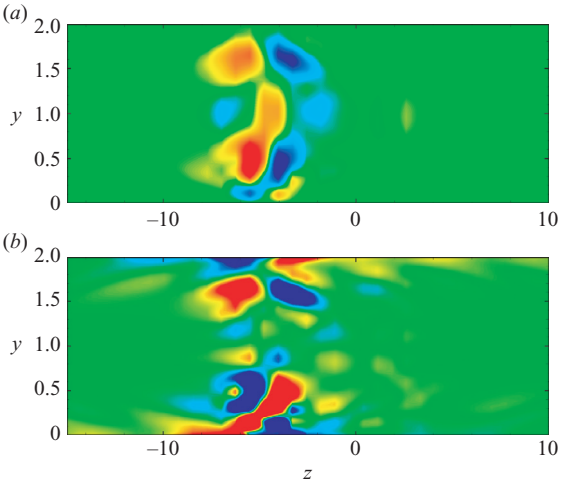

FIGURE 5. Contours of (*a*) $\partial w/\partial x$ and (*b*) the streamwise vorticity at $t = 120$ and $x = 40$ corresponding to structures A+B. Minimum and maximum levels in (*a*) and (*b*) are respectively ± 0.06 and ± 0.65. Positive and negative values are in red and blue, respectively.

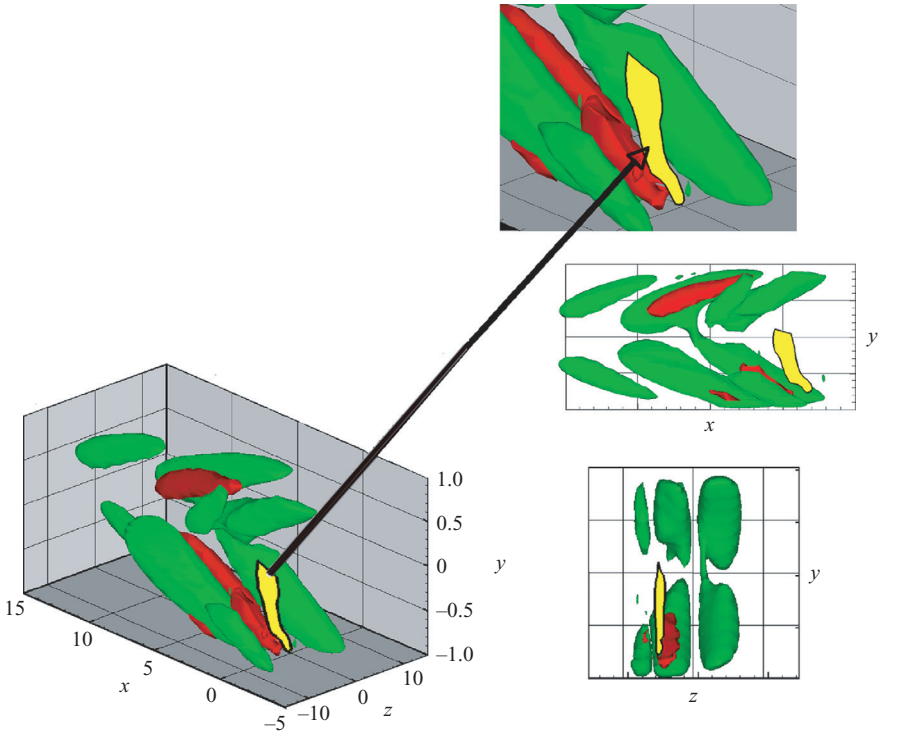

FIGURE 6. Regeneration of $\partial w/\partial x$ at $t = 10$. The birth of new wall-normal vorticity $\omega^*_{yn} = -\partial w/\partial x < 0$ is shown in yellow with intensity equal to -0.014. Red and green colours correspond to prevailing $\partial w/\partial x$ layers with $\partial w/\partial x = -0.01$ and 0.01.

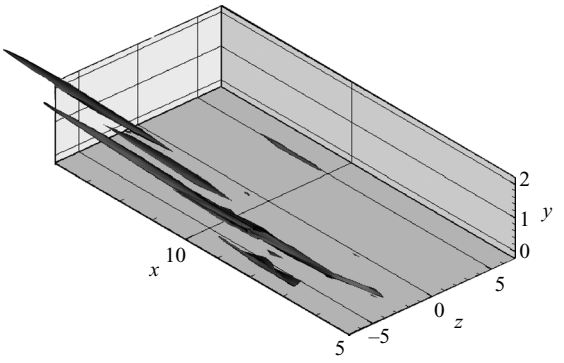

FIGURE 7. Quasi-streamwise vortices detected by $\lambda_2 = -0.01$ at $t = 22$.

The latter, which is predominantly streamwise, is stretched and can roll up into a new streamwise vortex because of a local unsteady separation resulting in regeneration of secondary vorticity at the wall. The rapidness of the ω^*_{yn} ejection observed here does certainly not result from this process, since otherwise B or A would also individually generate streamwise wall vorticity and this is not the case.

The snapshots in the (x, y)- and (z, y)-planes show that ω^*_{yn} is already partly tilted in the streamwise direction (figure 6). The tilting of ω^*_{yn} shear layers becomes streamwise stretching shortly after the triggering period. We adopted in Tardu & Nacereddine (2007) the Jiménez (1994) model that describes the longitudinal stretching stage through a Burgers' vorticity equation, and obtained good quantitative agreement for the elapse of time between the triggering of ω^*_{yn} and the appearance of the induced quasi-streamwise vortex. The streamwise stretching is almost completed at $t \approx 12$ and the generated structure is seen at this stage as a 'developed' quasi-streamwise vortex. This is more clearly seen in figure 7 that shows the λ_2 events detected at $t = 22$ and used to identify quasi-streamwise vortices (Jeong & Hussain 1995). More precise qualitative details on the development of these structures in time and space at their early stage of formation can be found in Tardu & Nacereddine (2007). The purpose of the present paper is to provide a quantitative analysis of the regeneration process and discuss its connection with the self-sustaining mechanisms of fully developed wall turbulence.

Some other initial perturbations have also been considered and gave similar results. In one case A was an axially symmetrical disturbance with the streamfunction

$$\psi_A = \varepsilon_A \, f(y) \, r^2 \, \exp[-(r/l_A)^2], \tag{13}$$

where $r = \sqrt{x^2 + z^2}$. The quasi-streamwise (QS) perturbation B has been spanwise shifted to interact with $\partial u/\partial z$ zones induced by this disturbance. Both perturbations were still individually stable. These configurations also lead to a local spot in a way closely similar to figure 4. The generic structures in the wall turbulence being QS, the emphasis is put on those structures.

5.2. *Parametric study*

A deeper comprehension of the interactive mechanism that we have introduced requires a detailed quantitative analysis. The strategy we adopted was to analyse the effect of one specific quantity on the process, keeping the others constant. Table 1 shows the parameters of the base configuration. The streamwise and spanwise length scales of structures A and B are kept constant together with the location of A, which

	Structure A $y_A = 1$	Structure B $y_B = 0.4$, $\delta_z = 6$
ε_p	0.1	0.02
l_x	4	2
l_z	4	2
p	2	1.5
q	2	6

TABLE 1. Parameters of the base configuration.

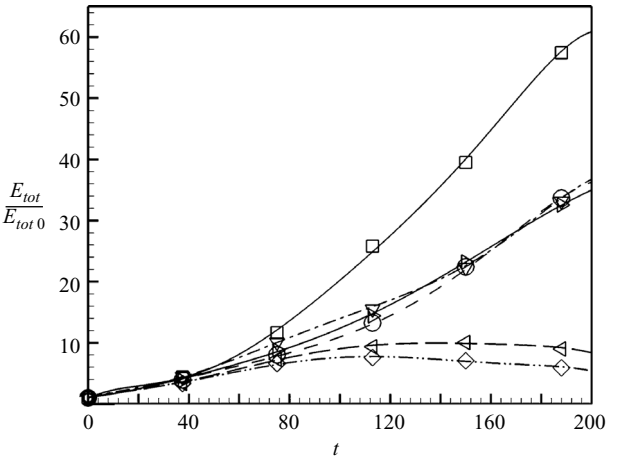

FIGURE 8. Total energy evolution for different values of the spanwise shift δ_z, versus time. δ_z: —□—, 2; ——○——, 3; —·—·▽·—·—·, 4;——▷——, 6;——◁——, 8; —··—··◇··—··—·, 12.

is at the centerline. The Reynolds number is fixed to $Re = 2000$. The spanwise shift δ_z, the distance of the structure B from the wall $a = y_B$, and the strengths ε_{pA} and ε_{pB} (figure 1) were changed in a large range and their effects have been analysed in detail.

The spanwise shift δ_z is varied from $\delta_z = 2$ to 12. Figure 8 shows the total energy versus time for different δ_z values. It is clearly seen that large spanwise shifts result in stable configurations because of the lack of interactions between A and B. Recall that the key to the regeneration mechanism is the compression (stretching) of the wall normal-vorticity $\omega_{y\pm A}$ patches by the sweep (ejection) events induced by B. Thus, either the left or the right vortex of the counter-rotating structure B has to 'touch' $\omega_{y\pm A}$ to trigger new ω^*_{yn}. Given that the spanwise extends of A and B are respectively $l_{zA} = 4$ and $l_{zB} = 2$, and that the distance of the right-hand B vortex to the symmetry line $z = 0$ is $d_B = \delta_z - l_{zB}/2$, B is outside the interaction zone when $\delta_z \gg (l_{zA} + l_{zB})/2 = 3$. Figure 9(*a*) and 9(*b*) show snapshots of the wall vorticity layers $\omega_{y\pm A}$ and $\omega_{y\pm B}$ at their initial stage of development ($t = 5$) for respectively $\delta_z = 3$ and $\delta_z = 8$. It is clearly seen that the interaction between A and B is weak in the latter case in which the structures evolve in time without communication, leading irreversably to a decrease of the energy E_t for $t > 100$. The temporal evolution of the energy E_v in the wall-normal velocity component shows that $\delta_z = 6$ is effectively a critical threshold and that the profiles approximately collapse for $3 \leqslant \delta_z \leqslant 6$ (figure 10). For $\delta_z \geqslant 6$, on the other hand, E_v hardly exceeds its initial value.

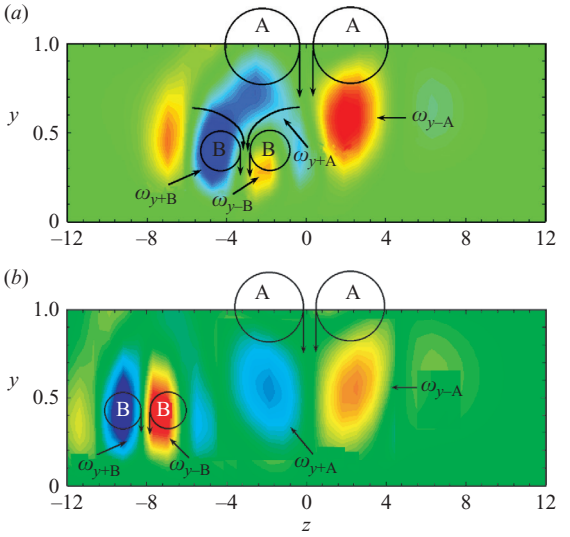

FIGURE 9. Snapshots of $\omega_y = \partial u/\partial z$ distribution at $t = 5$ for spanwise shifts (*a*) $\delta_z = 3$ and (*b*) $\delta_z = 8$. For $\delta_z = 3$, the vorticity values are typically $\omega_{y-A} \approx -0.04$ and $\omega_{y+A} \approx 0.02$, leading to the dissymmetry parameter $\Delta \approx 0.02$, while $\omega_{y-B} \approx -0.03$ and $\omega_{y+B} \approx 0.04$. For the large spanwise shift $\delta_z = 8$ in (*b*), $\omega_{y+A} \approx -\omega_{y-A} \approx 0.04$ and $\omega_{y+B} \approx -\omega_{y-B} \approx 0.06$, and the dissymmetry is $\Delta = 0$.

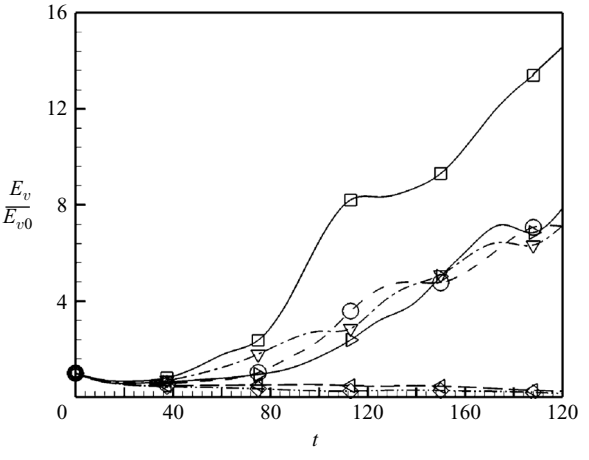

FIGURE 10. Evolution of the energy associated with the wall-normal velocity for different values of the parameter δ_z. For legend, see figure 8.

The vorticity layers $\omega_{y\pm A}$ and $\omega_{y\pm B}$ shown schematically in figure 1 are now clearly perceptible underneath the corresponding structures in figure 9(*b*). They develop independently in time and space for $\delta_z = 8$ and there is a perfect symmetry between the positive and negative wall layers. Consequently $\Delta = \partial\omega_{y+}/\partial x' - |\partial\omega_{y-}/\partial x'| \approx 0$ for both A and B and new $\partial w/\partial x$ layers cannot be triggered (see (5), § 2). The $\omega_{y\pm A}$ and $\omega_{y\pm B}$ patches diffuse and progressively disappear for longer times t, since the base configuration has been designed such that the individual structures are stable. The situation for smaller spanwise shift $\delta_z = 3$ is completely different (figure 9*a*). The

$\omega_{y+\mathrm{A}}$ layer associated with the left-hand counter-rotating vortex A is pushed left, and is destroyed beneath the structure under the straining stagnation flow induced by B. This action creates a strong asymmetry $\Delta = \partial\omega_{y+}/\partial x' - |\partial\omega_{y-}/\partial x'|$ that is as high as $\Delta = \frac{1}{2}\partial\omega_{y+}/\partial x'$ at $t = 5$. This results in the birth of ω^*_{yn}, which is subsequently tilted into elongated pseudo-turbulent structures (figure 7). Note that the intensity of the right-hand side $\omega_{y-\mathrm{A}}$ in figure 9(*a*) is effectively equal to its equivalent in figure 9(*b*) for $\delta_z = 8$, as expected, since both of them are far away from the interaction zone and are only under the effect of diffusion. Closer inspection of figure 9(*a*) also reveals an indirect influence of A on B, weakening $\omega_{y-\mathrm{B}}$ and reinforcing Δ, but this effect is only of secondary importance.

The vorticity in the compressed layer varies as $\omega_{y+A} \propto \exp(-\gamma_{\mathrm{B}}^+ t^+)$ and disappears rapidly for $t^+ \gg 2/\gamma_{\mathrm{B}}^+$ as discussed in detail in the previous section. Combining with the expression for the strain $\gamma_{\mathrm{B}}^+ = \pm\sqrt{3}Re_{\mathrm{B}}/(4a^{+2})$, results in the large upper limit of the set-up time $t_S^+ \gg a^{+2}/Re_{\mathrm{B}}$. It is interesting to note that a^{+2}/Re_{B} is also, incidentally, the time scale of the eruptive response induced by a convecting vortex near the wall (Walker 1989; Smith *et al.* 1991). The set-up time, on the other hand, has to be bounded and small compared with the algebraic instability time scale. Any initial perturbation gives rise to streaky structures under three-dimensional effects. The associated energy first increases up to typically the algebraic growth time scale $t_{\mathrm{Alg}} \approx 20$, but decreases subsequently due to viscous diffusion if it is not strong enough to trigger the bypass transition (Landahl 1980). The process we are discussing is intrinsically nonlinear, and in a way similar to a singular perturbation, the newly generated ω^*_{yn} layers have difficulty gaining enough strength to overcome the viscous diffusion if t_S^+ is too large. Thus, it is necessary that $t_S^+ < t_{\mathrm{Alg}}^+$, implying the condition $a^{+2}/Re_{\mathrm{B}} \ll t_S^+ < t_{\mathrm{Alg}}^+$. Therefore, B has to be close to the wall with a sufficiently high Reynolds number to trigger the interactive bypass transition, according to $Re_{\mathrm{B}}/a^{+2} > 1/t_{\mathrm{Alg}}^+$. Once this condition is fulfilled, similar arguments allow us to expect that the energy varies as $E_{tot} \propto Re_{\mathrm{B}}/a^{+2}$.

The Reynolds number of the structure B is directly proportional to the perturbation parameter, $Re_{\mathrm{B}} \propto \varepsilon_{p\mathrm{B}}$. Thus, to check the hypotheses that have been discussed, we first varied $\varepsilon_{p\mathrm{B}}$ in the range $0.001 \leqslant \varepsilon_{p\mathrm{B}} \leqslant 0.03$ keeping the rest of the parameters constant (table 1). The upper limit $\varepsilon_{p\mathrm{B}} = 0.03$ is chosen to maintain B stable. Figure 11 shows the temporal evolution of the total energy for different values of $\varepsilon_{p\mathrm{B}}$. The configuration is stable for $\varepsilon_{p\mathrm{B}} \leqslant 0.015$ and the energy increases in time suddenly for $\varepsilon_{p\mathrm{B}} \geqslant 0.015$. The existence of a triggering threshold is clearly perceptible in figure 12 that shows $E_{tot}/E_{tot\,0}$ versus $\varepsilon_{p\mathrm{B}}$ at $t = 200$. It is seen that the energy increases slowly until the critical value $\varepsilon_{p\mathrm{B}} = 0.015$ at which it jumps suddenly and increases rapidly immediately theseafter. It is also noteworthy that for $\varepsilon_{p\mathrm{B}} > 0.015$, there is a linear variation $E_{tot} \propto \varepsilon_{p\mathrm{B}}$ as predicted in the preceding paragraph. The line shown in figure 12 is deduced from a regression analysis with a coefficient close to 0.98.

Changing the parameter q_{B} in the (11) allows the control of the distance $y_{\mathrm{B}} = a$ of B from the wall. At $a \leqslant 0.30$ only the structure B becomes unstable. Accordingly, the location a has been varied in the range $0.30 \leqslant a \leqslant 0.67$. Figure 13 shows the $E_{tot}/E_{tot\,0}$ distribution versus time. It is seen that the configuration is stable until $a \geqslant 0.46$. The interactive mechanism becomes efficient and the energy increases rapidly in time, when the structure B is closer to the wall. Figure 14 shows $E_{tot}/E_{tot\,0}$ versus $1/a^2$ at $t = 200$ to check the validity of the conjecture $E_{tot} \propto Re_{\mathrm{B}}\, a^{+2}$ discussed above. There is effectively a linear relationship $E_{tot} \propto 1/a^2$ when $a \leqslant 0.46$ and the regression coefficient of the line shown in figure 14 is close to one. Moreover, the critical

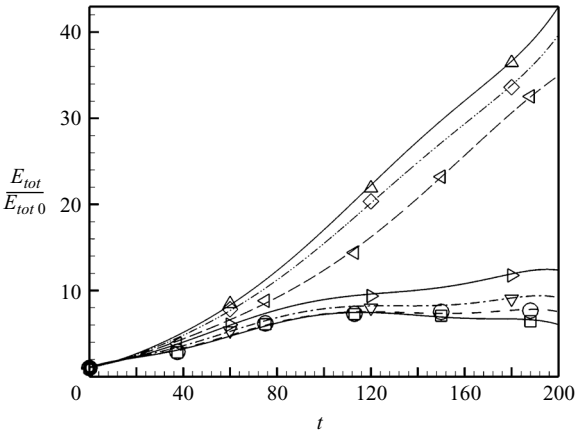

FIGURE 11. Energy evolution for different values of the strength of the structure B. ε_{pB}: —□—, 1×10^{-3}; -○—, 5×10^{-3}; ·—▽—·, 1×10^{-2}; —▷—, 1.5×10^{-2}; -◁—, 5×10^{-3}; 2×10^{-2}; ··—◇—·, 2.5×10^{-2}; —△—, 3×10^{-2}.

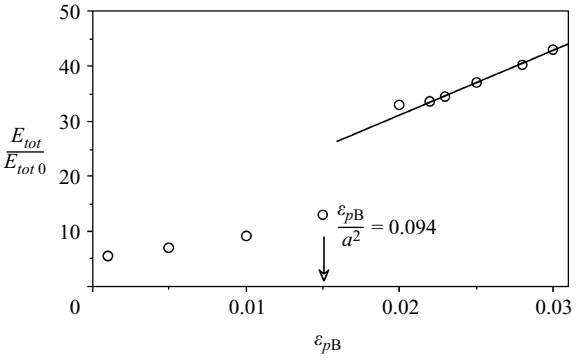

FIGURE 12. Energy versus the strength of the structure B at $t = 200$. The line is deduced from regression analysis.

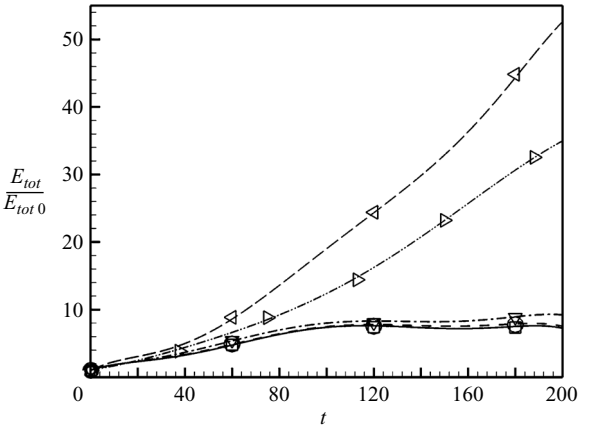

FIGURE 13. Energy versus time for different values of a the distance of the structure B from the wall. a: —□—, 0.67; -○—, 0.55; · —▽— ·, 0.46; —··—▷—·; 0.40; -◁—, 0.35.

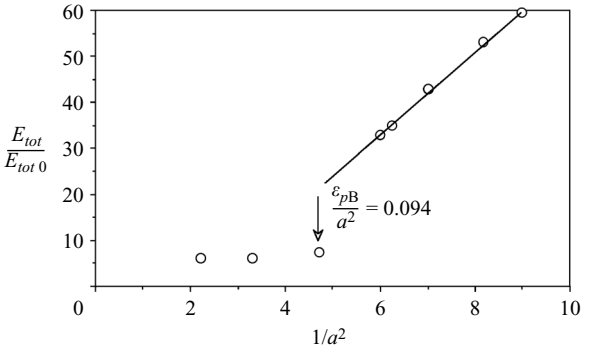

FIGURE 14. Evolution of the energy versus the inverse of the square of the distance of B from the wall at $t = 200$.

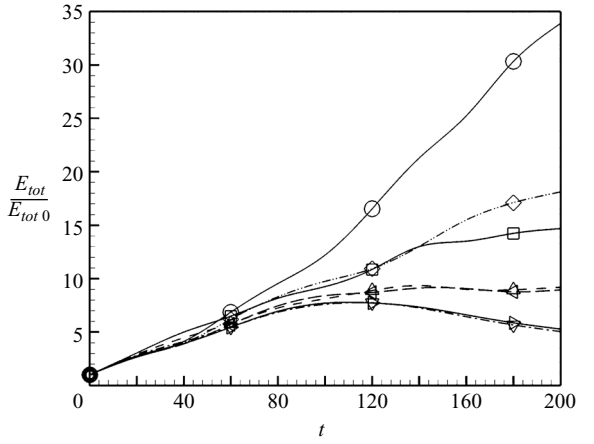

FIGURE 15. Total energy variation versus time for different values of $\varepsilon_{p\mathrm{A}}$ the intensity of the structure A. $\varepsilon_{p\mathrm{A}}$: —□—, 4×10^{-2}; -△—, 5×10^{-2}; · -▽- ·, 6×10^{-2}; —▷—, 7×10^{-2}; --◁—, 8×10^{-2}; -··—◇—·, 9×10^{-2}; —○—, 1×10^{-1}.

threshold parameter that triggers the bypass mechanism is $Re_{\mathrm{B}}/a^{+2} \propto \varepsilon_{p\mathrm{B}}/a^2 = 0.094$ obtained with $\varepsilon_{p\mathrm{B}} = 0.02$ ($Re_{\mathrm{B}} = 62$) and $a = 0.46$. One finds exactly the same value as in figure 13 in which we varied the intensity $\varepsilon_{p\mathrm{B}}$ while we kept $a = 0.4$, which clearly shows that Re_{B}/a^{+2} is a pertinent similarity parameter.

The asymmetry $\Delta = \partial\omega_{y+\mathrm{A}}/\partial x - |\partial\omega_{y-\mathrm{A}}/\partial x|$ appearing in (5) governs the genesis of new ω^*_{yn} patches. The initial $\omega_{y\pm\mathrm{A}}$ vorticity is connected to the intensity of the mother eddy A, since $Re_{\mathrm{A}} \propto \varepsilon_{p\mathrm{A}}$. The capacity of the generated $\partial w/\partial x$ layers to overcome the diffusion and give birth to small-scale quasi-streamwise vortices through tilting by the shear should therefore increase with $\varepsilon_{p\mathrm{A}}$. It is however difficult to precisely predict the way in which $\varepsilon_{p\mathrm{A}}$ triggers the transition, because of the strongly nonlinear character of the mechanism.

The intensity $\varepsilon_{p\mathrm{A}}$ was changed by a decade in the range $0.01 \leqslant \varepsilon_{p\mathrm{A}} \leqslant 0.1$. Figure 15 shows the $E_{tot}/E_{tot\,0}$ distribution versus time for different values of $\varepsilon_{p\mathrm{A}}$. The intensity in the $\omega_{y\pm\mathrm{A}}$ layers is roughly 0.04 for $\varepsilon_{p\mathrm{A}} = 0.07$, below which the combination is stable. The triggered $\partial w/\partial x$ layers are too weak at $\varepsilon_{p\mathrm{A}} \leqslant 0.07$ to generate quasi-streamwise vortices and a synthetic local turbulent layer that is reminiscent of the bypass transition. For larger $\varepsilon_{p\mathrm{A}}$, the strength of $\partial w/\partial x$ increases rapidly in time. To

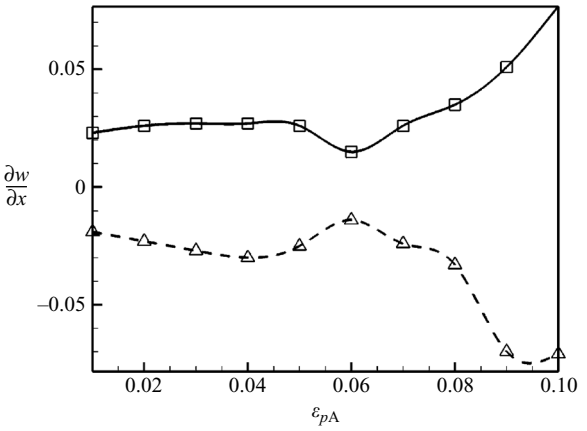

FIGURE 16. Maximum and minimum in the induced $\partial w/\partial x$ layers as a function of the intensity of the structure A. Maximum: —□—, minimum: – –△– –.

show this, we analysed the $\partial w/\partial x$ contours at $t = 200$ at a fixed distance $y = 0.6$ in the (x, z)-plane. We show in figure 16 the evolution of the minima and maxima of the $\partial w/\partial x$ contours as a function of the intensity ε_{pA}. The rapid increase of the $\partial w/\partial x$ activity for $\varepsilon_{pA} \geqslant 0.07$ is clearly perceptible in this figure. A power law $\partial w/\partial x \propto \varepsilon_{pA}^{n}$ with $n \approx 4$ describes the phenomena well, rather than a simple linear relationship.

The analysis conducted here confirms both qualitatively and quantitatively the key elements that we proposed in the § 2. The structures A and B have to be intense enough to trigger the regeneration mechanism. The spanwise shift δ_z of B with respect to A determines the spatial extend of the interaction zone. The closer the structure B is to the wall the faster the bypass transition.

6. Similarity with the regeneration process of the near-wall turbulent coherent structures

There are correspondences worth pointing out between the characteristics of the interactive bypass process and the self-sustaining mechanism of the near-wall turbulent coherent structures. The time scale of the regeneration process is $t_c \propto 2/\gamma$ where γ is the strain rate exerted by the pre-existing wall structures (§§ 3 and 5.2). The Reynolds number Re_{qs} of the quasi-streamwise vortices (QS) is approximately $Re_{qs} \approx 22$ according to the literature (Robinson 1991; Orlandi & Jiménez 1994). Most of the QS are concentrated in the buffer layer at a distance $a_{qs}^{+} = 20$ from the wall, where superscript + now refers to the quantities scaled by the inner variables, i.e. the viscosity ν and the shear velocity $u_\tau = \sqrt{\tau/\rho}$ with τ and ρ denoting respectively the wall shear stress and the density. Using these values gives $\gamma_{qs}^{+} = \sqrt{3}\, Re_{qs}/4a_{qs}^{+2} \approx 0.02$, resulting in $t_c^{+} \approx 100$ which is extremely close to the ejection period t_e^{+} in the buffer layer (Luchik & Tiederman 1987; Tardu 1995, 2002). The ejection period is the time between Reynolds-shear-stress-producing events and is connected to the so-called 'bursting' process. It should be interpreted as the regeneration time period in the present context.

The critical parameter $\chi = Re/a^2$ emerging from the analysis conducted in § 5.2 also has a clear physical meaning in the process governing the turbulent wall structures. Considering that the latter are regenerated when χ is larger than a critical value implies that the structures nearest to the wall (small a) are less intense (small Re)

than those that have reached larger distances and are mature. This is in agreement with some recent investigations (Zhou *et al.* 1999; Adrian, Meinhart & Tomkins 2000). The critical value of χ found in the bypass mechanism studied here is $\chi = 300$ (figures 12 and 14). The interactive bypass process leads to a turbulent spot with a local Reynolds number $Re_\tau = h\,u_\tau/\nu \approx 85$ at $t \geqslant 200$. The Re_τ has been determined by computing the shear stress velocity over the spot. It is slightly smaller than the $\mathrm{Re}_\tau = 90$ of fully turbulent channel flow at $Re = 2000$. Thus, the critical parameter in wall units triggering the bypass mechanism is $\chi^+ = Re/a^{+^2} = \chi/Re_\tau^2 = 0.04$, which is quite close to $\chi^+ = 0.055$ related to the quasi-streamwise vortices in the buffer layer ($Re = 22$ and $a^+ = 20$).

The streamwise vorticity intensity in the core of vortices is $|\omega_x| \approx 0.6$ at late stages of development (figure 6). That gives $|\omega_x|^+ \approx 0.14$ in wall units, which is in good agreement with the fully developed wall turbulence (Kim, Moin & Moser 1987). The streamwise extend of the wall structures varies between $\lambda_x^+ = 300$ and 400 and the spanwise distance between the streaks is about 100 wall units inside the spot. These values also compare quite well with the literature.

The initial intensity in the wall vorticity layers induced by the mother eddy A at the critical perturbation parameter $\varepsilon_{p\mathrm{A}} = 0.07$ that triggers the transition is $|\omega_{y\pm\mathrm{A}}| \approx |\partial u/\partial z| \approx 0.04$. This increases up to $|\omega_{y\pm\mathrm{A}}| \approx 0.18$ at $t = 10$, precisely when the new $\omega_{y\,n}^*$ patch is ejected from the wall (figure 7*a*). At this precise moment the spot has not yet developed and the inner scaling based on the laminar shear at the wall results in $|\omega_{y\pm\mathrm{A}}|^+ \approx 0.1$ which is small but not very different from the r.m.s. wall-normal vorticity fluctuations $\omega_y^+ \approx 0.15$ in the buffer layer at $y^+ = 10$ (Kim *et al.* 1987). The strength of the wall-layer vorticity contours varies between 0.1 and 0.2 in local wall units later, at $t \geqslant 100$, similarly to fully developed near-wall turbulence. The contribution of the $\partial w/\partial x$ term to ω_y^+ is limited to only 20 % in the spot, as expected, even though $\partial w/\partial x$ is at the origin of the bypass transition triggering mechanism.

The sign of induced wall-normal vorticity $\omega_{y\,n}^* < 0$ is opposite to the compressed layer $\omega_{y+\mathrm{A}}$ in the configuration given in figure 1. The $\omega_{y\,n}^*$ is tilted by the shear and subsequently stretched to give birth to a new quasi-streamwise structure with $\omega_{x\,new} < 0$, thus with sign opposite to the triggering structure $\omega_{x\,\mathrm{B}} > 0$ (figures 1 and 17*a*). Now, if the structure B has $\omega_{x\,\mathrm{B}} < 0$ the compression becomes stretching and the global effect is qualitatively similar giving rise to $\omega_{y\,n}^* > 0$ and $\omega_{x\,new} > 0$ according to (5) (figure 17*b*). That the effect of compression and stretching is roughly similar is perceptible in figure 18, which shows the temporal evolution of the total energy obtained simply by alternating the sign of $\varepsilon_{p\mathrm{B}}$. The resulting image of the process as a whole is a staggered array of vortices of alternating sign overlapping in the x-direction. This is similar to the scenario proposed by Jeong *et al.* (1997). The angle of the structures in the (x, y)-plane is about 10° and varies with the distance from the wall. That is also in agreement with these authors.

However, we could not clearly establish, at a first glance, a tilting between the structures in the horizontal (x, z)-plane either in the early or the late stages of their development, unlike to Jeong *et al.* (1997). These authors reported an angle of ± 4 between the coherent streamwise vortices in this plane. Kawahara *et al.* (1998) later related this phenomenon to the sinuous mode of streak instability. We first attributed this lack of tilting to the initial perturbation form, which is not initially tilted in the spanwise direction and the angle appearing in the perturbation streamfunctions is $\vartheta = 0$ in the present investigation. Imposing $\vartheta \neq 0$ increases the energy and facilitates the bypass transition during the transient algebraic period as clearly shown by Henningson *et al.* (1993). Closer inspection of all the data revealed, however, that the

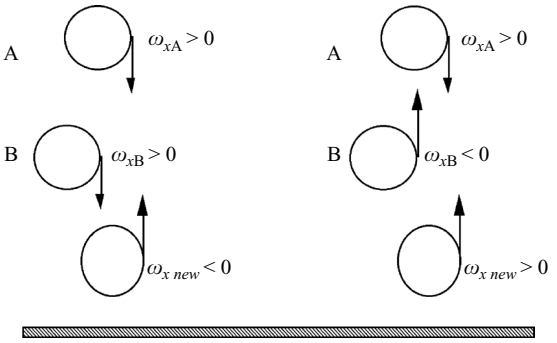

FIGURE 17. Generation of streamwise vortices of alternate sign.

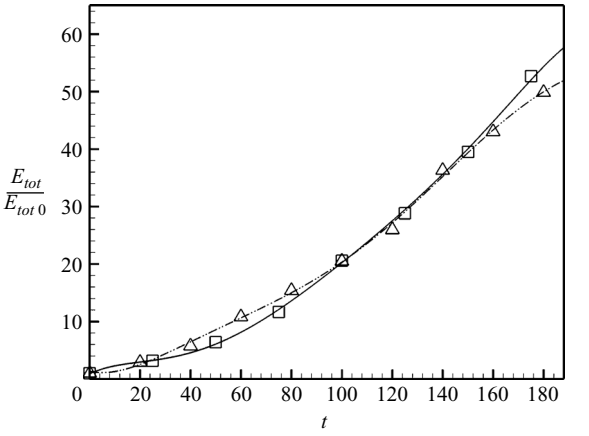

FIGURE 18. Evolution of the total energy associated with compression or stretching induced by the structure B for $\delta_z = 2$ and $\varepsilon_{pB} = \pm 0.02$. The rest of the parameters are given in table 1. Stretching: –··△··–··, compression: —□—.

structures do indeed become bented in the spanwise direction, typically at $20 < t < 50$, but that these phenomena are more difficult to observe later because of multiple breakup of the streaks. The spanwise shift δ_z also plays a role in the set-up of bending, although we can not yet clearly establish its effect. Figure 19 shows a snapshot of λ_2 contours at $t = 35$ and $t = 50$ obtained with $\delta_z = 4$. The streamwise vortex seen in figure 19(*a*) is effectively bented by 6° in the spanwise direction. After $t = 50$ however, there a rapid appearance of several small-scale vortices, and it is difficult to draw a clear conclusion about a systematic asymmetric organization of the structures (figure 19*b*).

In conclusion, there are some encouraging key elements showing that a mechanism similar to that proposed here might play a role in the regeneration of the near-wall coherent structures, at least partially. First, the generation of new structures is related to the effect of the primary ones by means of an interaction with pre-existing wall-normal vorticity layers by a somewhat deterministic scenario. The compression (stretching) of these patches of vorticity by the straining action of intense sweep (ejection) events triggers new wall-normal vorticity layers. They are tilted and subsequently stretched, the stretching becoming important at later stages. The arguments developed here predict correctly the location (on the sweep side underneath the mother eddy) and the rotational sign (opposite to that of the prevailing

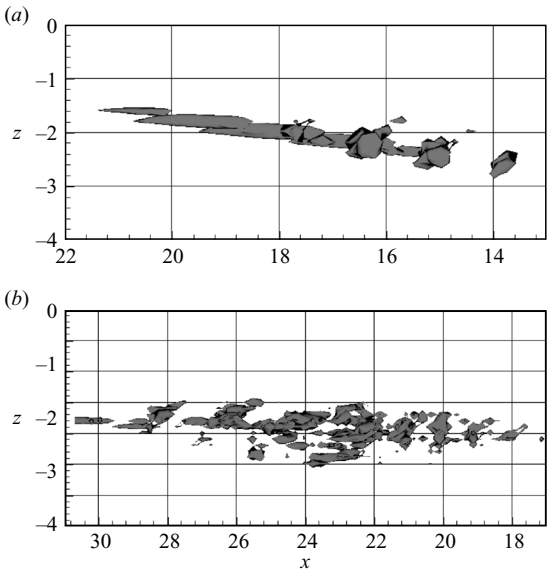

FIGURE 19. (*a*) A newly generated quasi-streamwise vortex is inclined in the spanwise direction at $t = 35$. (*b*) The tilting in the (x, z)-plane is difficult to detect in the presence of multiple break-up at $t = 50$. The spanwise shift is $\delta_z = 4$.

structure) of the offspring. This mechanism is strongly nonlinear and bypasses the linear instability and breakdown process of the streaks and their intrinsic subcritical instability. The time scale of the setting-up of the process depends upon the intensity of the primary vortices and the spanwise shift and it is typically $t_f \approx 8$. Scaling by the shear velocity of the base flow and the viscosity gives $t_f^+ = 16$. The set-up time scale is small compared to $t^+_{\partial u/\partial z} = 60$ which is the characteristic time associated with the inflectional instability due to the instantaneous spanwise variations $\partial u/\partial z$ of the fluctuating longitudinal velocity (Swearingen & Blackwelder 1987; Swearingen *et al.* 1987). The lifting of the wall-normal vorticity and the subsequent deviation from the two-dimensional configuration $u(y, z)$ towards $u(x, y, z)$ is a slow process with a characteristic time scale of about 100 wall units (Jiménez & Moin 1991). A different streak instability mechanism investigated recently by Schoppa & Hussain (2000, p. 852) revealed that the typical time of the linear transient growth of $w(x)$, suggested as a new generation mechanism of x-dependent flow near the wall, is about 30 wall units, which is still twice t_f^+. The rapid bypass mechanism should produce Reynolds-shear-stress events with comparatively small inter-arrival times. It has been known for some time that the so-called bursting process near the wall produces single and multiple ejections bursts called also packets (Tardu 1995, 2002; Zhou *et al.* 1999; Luchik & Tiederman 1987). The time separating two consecutive ejections within a packet is 20 wall units, which is 5 times smaller than the inter-arrival time of the single events. The total formation time of new structures including the birth of new wall-normal layers, their tilting and subsequent stretching is about $t_{tot} \approx 12$ which, non-dimensionalized by the inner variables of the base flow, becomes $t^+_{tot} \approx 25$. The rapid bypass transition of the wall streak instability should presumably lead to packets, while the single events would probably come from the linear three-dimensional instability process (Schoppa & Hussain 1997; Kawahara *et al.* 1998; Asai *et al.* 2002).

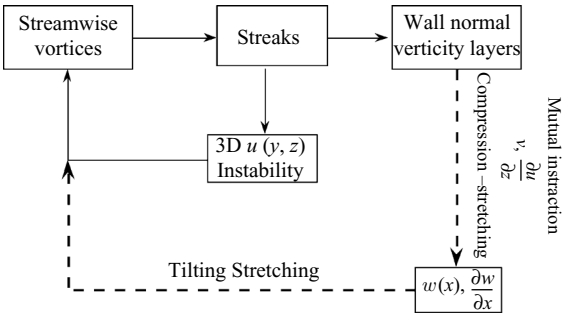

FIGURE 20. The consensual self-sustaining mechanism (continuous line) and its bypass (broken line).

The regeneration of the wall structures is a complex phenomenon including several different aspects and it is not claimed here that the mechanism we suggest constitutes the main or the major process. We only suggest that the classical three-dimensional linear streak instability and breakdown may be bypassed under some circumstances by the direct strong straining effect of the pre-existing structures, leading to rapid development of $w(x)$. We summarize in figure 20 the self-sustaining process suggested so far in solid lines (see for example Waleffe & Kim 1997; Jiménez & Pinelli 1999) together with the process bypassing the instability of $u(y, z)$ related to the streaks. The arguments here have to be checked in a fully developed turbulent wall flow, and this part of work is in progress. We have also shown recently that the regeneration process presented here can be successfully applied to micro-mixing in microchannel flows at significantly low Reynolds numbers through staggered unsteady wall jets shifted in the spanwise direction, as in figure 1 (Tardu & Nacereddine 2008).

7. Conclusion

The interaction between two disturbances of the form of streamwise vortices is investigated in a subcritical Poiseuille flow through direct numerical simulations at $Re = 2000$. The first disturbance A is passive, induces wall-normal vorticity layers through cinematic effects and its strength is not large enough to trigger the nonlinearity alone. The second structure B is designed in such a way that the straining effect it induces by means of sweep- (ejection) type events interacts with the wall-normal vorticity layers corresponding to the mother eddy. This structure is also individually stable. The compression (stretching) of these layers breaks the spanwise symmetry. A zone of a concentrated new wall-normal vorticity layer is consequently regenerated rapidly during a time period of the order of the outer time scale. This region is tilted by the mean shear, transformed into streamwise vorticity and rolls up into small-scale streamwise vortices. The process subsequently follows the classical route of bypass transition resulting in a localized turbulent spot.

The effects of the strength of the mother and triggering eddies A and B, the distance of B from the wall and the spanwise shift are analysed for fixed streamwise and spanwise scales of the structures. Varying the spanwise shift has clearly confirmed that the interactive bypass transition is caused by the breakdown of the spanwise symmetry, the spanwise shift determining the spatial extend of the interaction zone. The strengths of both A and B have to be large enough, first because the wall-normal vorticity layers they induce have to form intense zones and, secondly, they have to create strong straining flow. The similarity parameter χ defined as the ratio of the

Reynolds number of the disturbances to the square of their distance from the wall also has to be larger than a critical threshold. Two independent investigations, one conducted by modifying the intensity of the structures and the second by modifying their distances from the wall, resulted in the same critical χ value, showing the pertinence of this parameter.

A close similarity is found between the interactive bypass transition mechanism and the regeneration cycle of the turbulent wall structures by making use of quantities scaled with inner variables. The time scale of the process coincides well with the period of ejections in the buffer layer. The critical parameter χ in wall variables triggering the interactive bypass transition also corresponds well to the value related to the quasi-streamwise vortices in fully developed turbulent wall flow. The mechanism we propose results in staggered streamwise vortices of alternate sign, in agreement with several studies on wall turbulence. The streamwise and wall-normal vorticity intensity levels are in close agreement with the wall turbulence when they are properly scaled. One of the key elements of the regeneration process is the existence of the wall-normal vorticity layers surrounding the streaks and it is well known that their suppression breaks the self-sustaining cycle. These are some elements showing that the process suggested here might play some role in the self-sustaining mechanism near the turbulent wall. It can, for instance, bypass the three-dimensional instability of the streaks and can constitute at least part of the quasi-streamwise vortices generating process, which we believe results from an ensemble of different mechanisms rather than a unique cause-to-effect relationship.

The continuous support of IDRIS (Intensive Computational Facilities of National Scientific Research Center, CNRS) is warmly acknowledged.

The first author dedicates this paper to the memory of his father Esat Tardu.

REFERENCES

Adrian, R. J. 2007 Hairpin vortex organization in wall turbulence. *Phys. Fluids* **19**, 041301.

Adrian, R. J., Meinhart, C. D. & Tomkins, C. D. 2000 Vortex organization in the outer region of the turbulent boundary layer. *J. Fluid Mech.* **422**, 1–53.

Asai, M., Minagawa, M. & Nishioka, M. 2002 The instability and breakdown of a near wall low-speed streak. *J. Fluid Mech.* **455**, 289–314.

Bakchinov, A. A., Westin, K. J., Kozlov, V. V. & Alfredsson, P. H. 1998 Experiments on localized disturbances in a plate boundary layer. Part 2. Interaction between localized disturbances and T-S waves. *Eur. J. Mech.* B/*Fluids* **17**, 847–873.

Bech, K. H., Henningson, D. S. & Henkes, R. W. M. 1998 Linear and nonlinear development of localized disturbances in zero and adverse pressure gradient boundary layer. *Phys. Fluids* **10**, 1405–1418.

Bernard, P.-S., Thomas, J.-M. & Handler, R.-A. 1993 Vortex dynamics and the production of Reynolds stress. *J. Fluid Mech.* **253**, 385–419.

Brooke, J.-W. & Hanratty, T. J. 1993 Origin of turbulence-producing eddies in a channel flow. *Phys. Fluids* A **5**, 1011–.

Butler, K. M. & Farrell, B. F. 1992 Three-dimensional optimal perturbations in viscous shear flow. *Phys. Fluids* A **4**, 1637–.

Corcos, G. M. & Shermann, F. S. 1984 The mixing layer: deterministic models of a turbulent flow. Part 1. Introduction and the two-dimensional flow. *J. Fluid Mech.* **139**, 29–65.

Doligalski, T. L. & Walker, J. D. A. 1984 The boundary layer induced by a convected two-dimensional vortex. *J. Fluid Mech.* **139**, 1–28.

Gustavsson, L. H. 1991 Energy growth of three-dimensional disturbances in plane Poiseuille flow. *J. Fluid Mech.* **224**, 241–260.

Hamilton, J. M., Kim, J. & Waleffe, F. 1995 Regeneration mechanism of near-wall turbulence structures. *J. Fluid Mech.* **287**, 317–348.

Henningson, D. S., Lundbladh, A. & Johansson, A. 1993 A mechanism for bypass transition from localized disturbances in wall-bounded shear flows. *J. Fluid Mech.* **250**, 169–207.

Jeong, J. & Hussain, F. 1995 On the identification of a vortex. *J. Fluid Mech.* **285**, 69–94.

Jeong, J., Hussain, F., Schoppa, W. & Kim, J. 1997 Coherent structures near the wall in a turbulent channel flow. *J. Fluid Mech.* **332**, 185–214.

Jiménez, J. 1992 Kinematic alignment effects in turbulent flows. *Phys. Fluids* A **4**, 652–

Jiménez, J. 1994 On the structure and control of wall turbulence. *Phys. Fluids* **6** 944–953.

Jiménez, J. & Moin, K. 1991 The minimal flow unit in near wall turbulence. *J. Fluid Mech.* **225**, 213–240.

Jiménez, J. & Orlandi, P. 1993 The roll-up of a vortex layer near a wall. *J. Fluid Mech.* **248**, 297–313.

Jiménez, J. & Pinelli, A. 1999 The autonomous cycle of near-wall turbulence. *J. Fluid Mech.* **389**, 335–359.

Kawahara, G., Jiménez, J., Uhlmann, M. & Pinelli, A. 1998 The instability of streaks in near wall turbulence. *Annual Research Briefs, Center for Turbulence Research, Stanford*, pp. 155–170.

Kim, J., Moin, P. & Moser, R. 1987 Turbulence statistics in fully developed channel flow at low Reynolds number. *J. Fluid Mech.* **177**, 133–166.

Landahl, M. T. 1980 A note on an algebraic instability of inviscid parallel shear flows. *J. Fluid Mech.* **98**, 243–251.

Luchik, T. S. & Tiederman, W. G. 1987 Timescale and structure of ejections and bursts in turbulent channel flows. *J. Fluid Mech.* **174**, 529–552.

Matsubara, M., Bakchinov, A. A., Fransson, J. H. & Alfredsson, P. H. 2000 Growth and breakdown of streaky structures in boundary-layer transition induced by freestream turbulence. In *Laminar-Turbulent Transition* (ed. H. Fasel & W. Saric), pp. 371–376. Springer.

Morkovin, M. V. 1969 The many faces of transition. In *Viscous Drag Reduction* (ed. C. S. Wells). Plenum.

Orlandi, P. 2001 *Fluid Flow Phenomena. A Numerical Toolkit*. Kluwer.

Orlandi, P. & Jiménez, J. 1994 On the generation of turbulent wall friction. *Phys. Fluids* **6**, 634.

Reddy, S. C. & Henningson, D. S. 1993 Energy growth in viscous channel flows. *J. Fluid Mech.* **252**, 209–238.

Robinson, S.-K. 1991 The kinematics of turbulent boundary layer structure. *NASA Tech. Mem.* 103859.

Sankaran, R., Sokolov, M. & Antonia, R. A. 1998 Substructures in a turbulent spot. *J. Fluid Mech.* **197**, 389–414.

Schoppa, W. & Hussain, F. 1997 Genesis and dynamics of coherent structures in near-wall turbulence: a new look. In *Self-Sustaining Mechanisms of Wall Turbulence* (ed. R. L. Panton), pp. 385–422. Computational Mechanics Publications, Southampton.

Schoppa, W. & Hussain, F. 2000 Generation of near-wall coherent structures in a turbulent boundary layer. *Current Sci*, **79**, 849–858.

Sendstad, O. & Moin, P. 1992 The near wall mechanics of three-dimensional turbulent boundary layers *Stanford Univ. Dept. of Mech. Engineering, Thermosciences Div. Rep.* TF-57.

Smith, C. R., Walker, J. D. A, Haidari, A. H. & Sobrun, U. 1991 On the dynamics of near wall turbulence. *Phil. Trans. R. Soc. Lond.* A **336**, 131

Swearingen, J. D., Blackwelder, R. F. 1987 The growth and breakdown of streamwise vortices in the presence of the wall. *J. Fluid Mech.* **182**, 255–290.

Swearingen, J. D., Blackwelder, R. F. & Spalart, P.-R. 1987 Inflectional instabilities in the wall region of bounded turbulent shear flows. *Report* CTR-S87, pp. 291–295.

Tardu, S. 1995 Characteristics of single and clusters of bursting events in the inner region of a turbulent channel flow; Part 1: Shear layer events. *Exps. Fluids* **20**, 112–124.

Tardu, S. 1995 Coherent structures and riblets. *Appl. Sci. Res.* **54**, 349–385.

Tardu, S. 2002 Characteristics of single and clusters of bursting events in the inner region of a turbulent channel flow; Part 2: Level crossing events. *Exps. Fluids* **33**, 640–652.

Tardu, S. & Nacereddine, R. 2007 Bypass transition through interactions of localized disturbances in wall bounded flows. *J. Non-linear Dyna.* **50**, 767–779.

Tardu, S. & Nacereddine, R. 2008 A new active micromixing strategy. *Heat Transfer Engng* (to appear).

Waleffe, F. & Kim, J. 1997 How streamwise rolls and streaks self-sustain in a shear flow. In *Self-Sustaining Mechanisms of Wall Turbulence* (ed. R. L. Panton), pp. 309–332, Computational Mechanics Publications, Southampton.

Walker, J. D. A. 1989 Wall layer eruptions in turbulent flows. In *2nd IUTAM Symp. on Structure of Turbulence and Drag Reduction* (ed. A. Gyr), pp. 59–67 Springer; also *NASA Tech. Memo.* 102362, ICOMP-89–26.

Westin, K. J. A., Bakchinov, A. A., Kozlov, V. V. & Alfredsson, P. H. 1998 Experiments on localized disturbances in a plate boundary layer. Part 1. The receptivity and evolution of a localized free stream disturbance. *Eur. J. Mech.* B/*Fluids* **17**, 823–846.

Zhou, J., Adrian, R. J., Balachandar, S. & Kendall, T. M. 1999 Mechanisms for generating coherent packets of hairpin vortices in channel flow. *J. Fluid Mech.* **387**, 353–396.